Dyes and Pigments 190 (2021) 109320

Contents lists available at ScienceDirect

Dyes and Pigments

journal homepage: http://www.elsevier.com/locate/dyepig

Effect of conjugation on the optoelectronic properties of pyrazine-based push-pull chromophores: Aggregation-induced emission, solvatochromism, and acidochromism

Hyung-Ha Park [1], Puttavva Meti [1], Young-Dae Gong [*]

Innovative Drug Library Research Center, Department of Chemistry, College of Science, Dongguk University, 26, 3-ga, Pil-dong, Jung-gu, Seoul, 04620, South Korea

ARTICLE INFO

Keywords:
Pyrazine
Aggregation-induced emission
Charge transfer
Solvatochromism

ABSTRACT

A series of pyrazine-based bipodal D-π-A-π-D and D-π-A-π-A molecules with multi-stimuli response have been synthesized via Suzuki and Sonogashira cross-coupling reactions. We present a joint theoretical and experimental study to elucidate structure-property relationship of these push-pull chromophores. The modification of the end-capped donor-acceptor units and the extension of π-conjugation are key factors in tuning their optical, thermal and electrochemical properties. Depending on the different electron-donating substituents, the chromophores emit blue to orange fluorescence. The solvent dependent emission was observed and their Dimroth-Reichardt plots show a linear correlation. The aggregation-induced study shows enhanced emission in aggregates. Our work has elucidated that these small structural isomers can be utilized to develop a promising multi-stimuli responsive fluorescent materials.

1. Introduction

The development of efficient organic luminophoric materials is a frontier area of research, due to their extensive applications in biomedical [1,2], optoelectronics [3,4], and sensors [5–8]. Understanding how molecular structures and conformations of molecules affect their photophysical processes in the solid state is a prerequisite for the rational design of new luminophoric systems [9]. Many conventional materials in their dilute solutions are highly emissive. However, most of the organic luminescent materials in solid state are nonfluorescent, due to the aggregation-caused quenching (ACQ) [10,11]. Thus, luminescent materials, which can overcome this emission quenching problem or even show enhanced emission in solid state, would be very rewarding. Modulation of the solid-state optical properties of luminophores has technological implications because the materials are commonly used as solid thin films for their real-world applications in electronic and photonic devices. Researchers have paid a lot of attention to organic chromophores bearing electron donor and acceptor groups linked by π-conjugated bridges, owing to their appealing optical response. The optical properties of luminophors can be finely tuned by selecting appropriate donor (D), acceptor (A), and π-bridges at suitable positions [12]. The interaction between conjugation and D-A group is the most important factors in determining the properties of molecules, and understanding these relationships is vital to synthesize ideal luminogens.

Great efforts have been dedicated to the development of novel organic fluorophore with aggregation-induced emission (AIE) properties [13], since its first report by Tang and co-workers in 2001 [14]. Aggregation strongly affects the optical properties of dyes, making them good probes for fluorescence microscopy and *in vivo* imaging [15–17]. AIEgens with versatile functionalities and diverse applications have been reported. But most of them are aromatic hydrocarbons, such as tetraphenylethenes [18–20], styrylbenzenes [21–23], and arylbenzenes [24]. The development of novel AIE-active molecules has become a hot research topic. To enrich the AIE-active molecules with a wide range of emission colors, one of the most important methods is to incorporate heteroatom into the AIE skeleton to construct D-A structure [25]. Also, the insertion of heteroatom into conjugated backbone provides non-covalent interactions. Very few pyrazine-containing chromophores with AIE properties have been reported [26–29]. Nevertheless, there is huge space to modify the structure, and to develop pyrazine-based materials. Pyrazines have emerged as a leading class of functionalized materials, due to their facile synthesis and flexible structure modification [30]. Pyrazine with its strong electron-deficient character is commonly connected to π-linker into push-pull system that favors the intramolecular

* Corresponding author.
E-mail address: ydgong@dongguk.edu (Y.-D. Gong).
[1] Hyung-Ha Park and Puttavva Meti contributed equally to this work.

https://doi.org/10.1016/j.dyepig.2021.109320
Received 30 December 2020; Received in revised form 3 March 2021; Accepted 14 March 2021
Available online 18 March 2021

charge transfer (ICT) [31–34]. Motivated by the attractive potentials of these pyrazine derivatives in electronic devices, such as organic light-emitting diodes [35], photovoltaic cells [36], and field effect transistors [37], we have been engaged in the synthesis of pyrazine-based push-pull molecules to explore AIE properties.

In continuation of our research interests on luminescent materials [38,39], we have synthesized a series of linear and V-shaped pyrazine based push-pull chromophores with D-π-A-π-D and D-π-A-π-A structural configurations (Fig. 1). These chromophores feature pyrazine as a central electron acceptor unit and benzene rings as π-linker with the pendant donor (NMe_2, NPh_2, and carbazole) and acceptor groups (CF_3, OCF_3, CN, and NO_2). We mainly focus on the viewpoint of how molecular conformations and the nature of functional groups affect the photophysical and electrochemical properties of the resulting molecules. The introduction of appropriate electron donor and acceptor into the phenyl ring effectively tunes the range of emission colors of the resulting dipolar compounds. The optical, thermal, electrochemical properties and AIE characteristics were carefully investigated which show strong D-A interaction. Furthermore, the experimental studies were supported by density functional theory (DFT) calculations. We propose that the different optical behaviors are related to their molecular structures. The results indicate that these pyrazine derivatives show strong emission solvatochromism, acidochromism and AIE properties.

2. Experimental section

2.1. Materials and instrumentation

All reagents and catalyst were used as received unless otherwise indicated. Column chromatography was carried out using silica gel 60 (0.040–0.063 mm Merck). Nuclear magnetic resonance (^{1}H NMR and ^{13}C NMR) spectra were obtained by Bruker-500 MHz spectrometry in $CDCl_3$ solutions. High-resolution mass spectra (HR-MS) were obtained using a Q-TOF LC/MS system. Melting points were measured using Stuart SMP40 melting point apparatus. Microwave reactions were conducted by using Biotage initiator microwave system.

The UV–vis absorption spectra were measured by Varian cary-50 spectrophotometer and photoluminescence (PL) spectra were carried out by Cary Eclipse Fluorescence Spectrophotometer. Both UV absorption and emission spectra was recorded using standard 1 cm quartz cell. Thermogravimetric analysis (TGA) and differential scanning calorimetry (DSC) were measured under nitrogen at a heating rate of 10 °C per minute with STA 6000 and Perkin Elmer-Jade. Cyclic voltametric measurements (CV) were performed using a ZIVE MPI Electrochemical Workstation. A three-electrode system was used with Pt as a working electrode, Ag wire as a reference electrode, Pt wire as a counter electrode and 0.1 M tetrabutylammonium hexafluorophosphate ($TBAPF_6$) was used as a supporting electrolyte.

General method for the synthesis of precursors (A). A mixture of 2,5-dibromopyrazine (**1**) (2 g, 8.4 mmol), $Pd(PPh_3)_4$ (10 mol%), 2 M K_2CO_3 (10 mL) and 4-bromophenyl boronic acid (3.37 g, 16.8 mmol) are dissolved in toluene (50 mL) and ethanol (10 mL). The reaction mixture was stirred at 70 °C for 14 h under nitrogen atmosphere. After being cooled, the reaction mixture was diluted with water and extracted with CH_2Cl_2 (3 × 30 mL). The combined organic layer was washed with water and dried with anhydrous $MgSO_4$. Then solvent was evaporated in vacuum, and the residues were purified by silica gel column chromatography using hexane/ethyl acetate (10:1, v/v) to get the desired compound **2**. Similarly, precursor **6** was obtained using 2,6-dibromopyrazine (**5**).

2,5-bis(4-bromophenyl)pyrazine (2). Yield: 2.33 g (71%); white powder. ^{1}H NMR (500 MHz, $CDCl_3$) δ 9.04 (s, 2H), 7.95 (d, J = 8.3 Hz, 4H), 7.66 (d, J = 8.3 Hz, 4H). ^{13}C NMR (126 MHz, $CDCl_3$) δ 149.88, 140.96, 135.01, 132.32, 128.28, 124.57. HRMS (ESI) m/z; $[M+H]^+$ Calcd for $C_{16}H_{10}Br_2N_2$, 388.9284; found 388.9284.

2,6-bis(4-bromophenyl)pyrazine (6). Yield: 2.85 g (87%); white powder. ^{1}H NMR (500 MHz, $CDCl_3$) δ 8.96 (s, 2H), 8.01 (d, J = 8.5 Hz, 4H), 7.67 (d, J = 8.5 Hz, 4H). ^{13}C NMR (126 MHz, $CDCl_3$) δ 150.60, 139.92, 135.18, 132.27, 128.52, 124.73. HRMS (ESI) m/z; $[M+H]^+$ Calcd for $C_{16}H_{10}Br_2N_2$, 388.9284; found 388.9281.

Mono-coupled products **3** and **7** were synthesized according to the general procedure (A) using one equivalent of (4-(diphenylamino) phenyl)boronic acid under microwave irradiation at 65 °C for 15 min.

4'-(5-(4-bromophenyl)pyrazin-2-yl)-*N,N*-diphenyl-[1,1′-biphenyl]-4-amine (3). Yield: 1.23 g (48%); pale yellow powder. ^{1}H NMR (500 MHz, $CDCl_3$) δ 9.11 (s, 1H), 9.06 (s, 1H), 8.13 (d, J = 8.1 Hz, 2H), 7.96 (d, J = 8.3 Hz, 2H), 7.74 (d, J = 8.1 Hz, 2H), 7.67 (d, J = 8.3 Hz, 2H), 7.55 (d, J = 8.4 Hz, 2H), 7.29 (t, J = 7.7 Hz, 4H), 7.20–7.12 (m, 6H), 7.06 (t, J = 7.2 Hz, 2H). ^{13}C NMR (126 MHz, $CDCl_3$) δ 150.71, 149.37, 147.79, 147.56, 142.17, 141.14, 140.95, 135.26, 134.39, 133.78, 132.29, 129.35, 128.24, 127.74, 127.19, 127.18, 124.66, 124.35, 123.62, 123.20. HRMS (ESI) m/z; $[M+H]^+$ Calcd for $C_{34}H_{24}BrN_3$, 554.1227; found 554.1200.

4'-(6-(4-bromophenyl)pyrazin-2-yl)-*N,N*-diphenyl-[1,1′-biphenyl]-4-amine (7). Yield: 1.31 g (51%); pale yellow powder. ^{1}H NMR (500 MHz, $CDCl_3$) δ 9.01 (s, 1H), 8.93 (s, 1H), 8.20 (d, J = 8.2 Hz, 2H), 8.05 (d, J = 8.4 Hz, 2H), 7.74 (d, J = 8.2 Hz, 2H), 7.67 (d, J = 8.3 Hz, 2H), 7.55 (d, J = 8.5 Hz, 2H), 7.29 (t, J = 7.8 Hz, 4H), 7.16 (m, 6H), 7.06 (t, J = 7.3 Hz, 2H). ^{13}C NMR (126 MHz, $CDCl_3$) δ 151.34, 150.46, 147.77, 147.53, 142.28, 140.11, 139.38, 135.44, 134.53, 133.75, 132.20, 129.34, 128.53, 127.74, 127.40, 127.10, 124.64, 124.54, 123.59, 123.18. HRMS (ESI) m/z; $[M+H]^+$ Calcd for $C_{34}H_{24}BrN_3$, 554.1227; found 554.1214.

General procedure for synthesis compounds 4(b-c) and 8(a-c). A mixture of compound 2,5-bis(4-bromophenyl)pyrazine (**2**) (300 mg, 0.77 mmol) was dissolved in toluene (2 mL) and ethanol (1 mL), subsequently, $Pd(PPh_3)_4$ (10 mol%), corresponding boronic acid (1.93 mmol) and 2 M K_2CO_3 (1.2 mL) were added and the reaction mixture was irradiated in a MW at 80 °C for 1 h. After cooling to RT, the reaction mixture was quenched with water and extracted CH_2Cl_2 (3 × 10 mL). The combined organic layer was washed with water and dried with $MgSO_4$. The solvent was removed by vacuum distillation, and the residues were purified by silica column chromatography (ethyl acetate/hexane, 10:1, v/v) to afford final products **4(b-c)**. Similarly, compounds **8(a-c)** were prepared using 2,6-bis(4-bromophenyl)pyrazine (**6**).

4′,4‴-(pyrazine-2,5-diyl)bis(*N,N*-diphenyl-[1,1′-biphenyl]-4-amine) (4b). Yield: 360 mg (65%); pale yellow powder, m.p: 282–284 °C. ^{1}H NMR (500 MHz, $CDCl_3$) δ 9.13 (s, 2H), 8.14 (d, J = 8.4 Hz, 4H), 7.74 (d, J = 8.4 Hz, 4H), 7.56 (d, J = 8.6 Hz, 4H), 7.29 (t, J = 7.9 Hz, 8H), 7.16 (m, 12H), 7.06 (t, J = 7.3 Hz, 4H). ^{13}C NMR (126 MHz, $CDCl_3$) δ 150.16, 147.71, 147.56, 141.95, 141.12, 134.61, 133.87, 129.34, 127.73, 127.15, 127.12, 124.62, 123.65, 123.15. HRMS (ESI) m/z; $[M+H]^+$ Calcd for $C_{52}H_{38}N_4$, 719.3170; found 719.3146.

2,5-bis(4'-(9H-carbazol-9-yl)-[1,1′-biphenyl]-4-yl)pyrazine (4c). Yield: 187 mg (34%); off white powder, m.p: 320–322 °C. ^{1}H NMR (500 MHz, $CDCl_3$) δ 9.21 (s, 2H), 8.26 (d, J = 7.9 Hz, 4H), 8.18 (d, J = 7.6 Hz, 4H), 7.92 (d, J = 8.0 Hz, 4H), 7.89 (d, J = 8.0 Hz, 4H), 7.71 (d, J = 7.9 Hz, 4H), 7.51 (d, J = 8.0 Hz, 4H), 7.45 (t, J = 7.5 Hz, 4H), 7.32 (t, J = 7.3 Hz, 4H). ^{13}C NMR (126 MHz, $CDCl_3$) δ 150.27, 141.64, 141.30, 140.84, 139.33, 137.43, 135.52, 128.53, 127.80, 127.48, 127.40, 126.03, 123.53, 120.38, 120.09, 109.84. HRMS (ESI) m/z; $[M+H]^+$ Calcd for $C_{52}H_{34}N_4$, 715.2857; found 715.2836.

4′,4‴-(pyrazine-2,6-diyl)bis(*N,N*-dimethyl-[1,1′-biphenyl]-4-amine) (8a). Yield: 265 mg (73%); yellow powder, m.p: 264–266 °C. ^{1}H NMR (500 MHz, $CDCl_3$) δ 8.97 (s, 2H), 8.22 (d, J = 6.8 Hz, 4H), 7.74 (d, J = 6.0 Hz, 4H), 7.61 (d, J = 7.2 Hz, 4H), 6.84 (d, J = 6.5 Hz, 4H), 3.03 (s, 12H). ^{13}C NMR (126 MHz, $CDCl_3$) δ 151.41, 150.31, 142.67, 139.36, 134.10, 128.10, 127.74, 127.35, 126.60, 112.74, 40.53. HRMS (ESI) m/z; $[M+H]^+$ Calcd for $C_{32}H_{30}N_4$, 471.2543; found 471.2539.

4′,4‴-(pyrazine-2,6-diyl)bis(*N,N*-diphenyl-[1,1′-biphenyl]-4-amine) (8b). Yield: 465 mg (84%); pale yellow powder, m.p: 202–204 °C. ^{1}H NMR (500 MHz, $CDCl_3$) δ 9.00 (s, 2H), 8.23 (d, J = 8.3 Hz, 4H), 7.75 (d, J = 8.3 Hz, 4H), 7.56 (d, J = 8.5 Hz, 4H), 7.29 (t, J =

7.8 Hz, 8H), 7.16 (m, 12H), 7.05 (t, $J = 7.3$ Hz, 4H). ^{13}C NMR (126 MHz, $CDCl_3$) δ 151.23, 147.70, 147.55, 142.11, 139.60, 134.83, 133.89, 129.33, 127.74, 127.40, 127.07, 124.61, 123.63, 123.15. HRMS (ESI) *m/z*; $[M+H]^+$ Calcd for $C_{52}H_{38}N_4$, 719.3170; found 719.3157.

2,6-bis(4'-(9H-carbazol-9-yl)-[1,1′-biphenyl]-4-yl)pyrazine (8c). Yield: 429 mg (78%); off white powder, m.p: 312–314 °C. ^{1}H NMR (500 MHz, $CDCl_3$) δ 9.09 (s, 2H), 8.35 (d, $J = 8.3$ Hz, 4H), 8.17 (d, $J = 7.7$ Hz, 4H), 7.92 (d, $J = 8.4$ Hz, 4H), 7.90 (d, $J = 8.4$ Hz, 4H), 7.70 (d, $J = 8.4$ Hz, 4H), 7.51 (d, $J = 8.2$ Hz, 4H), 7.45 (t, $J = 7.6$ Hz, 4H), 7.32 (t, $J = 7.4$ Hz, 4H). ^{13}C NMR (126 MHz, $CDCl_3$) δ 151.19, 141.78, 140.80, 140.00, 139.34, 137.42, 135.74, 128.54, 127.74, 127.66, 127.46, 126.02, 123.50, 120.38, 120.09, 109.83. HRMS (ESI) *m/z*; $[M+H]^+$ Calcd for $C_{52}H_{34}N_4$, 715.2857; found 715.2836.

General procedure for the synthesis of compounds 4(d-h) and 8 (d-h). Monosubstituted compound **3** (300 mg, 0.54 mmol), $Pd(PPh_3)_4$ (10 mol%), corresponding boronic acid (0.70 mmol) and 2 M K_2CO_3 (1 mL) were dissolved in toluene (2 mL) and ethanol (1 mL). Then the reaction mixture was stirred at 80 °C for 1 h under MW. After cooling to RT, the solvent was evaporated in vacuum. The reaction mixture was quenched with water and extracted CH_2Cl_2 (3 × 10 mL). The combined organic layer was washed with water and dried with $MgSO_4$. The solvent was removed using a rotary evaporator, and the residue was purified by column chromatography (ethyl acetate/hexane, 10:1, v/v) to afford the desired linear compounds **4(d-h)**. Similarly, bent shaped compounds **8(d-h)** were prepared using compound **7** with the corresponding boronic acids.

***N,N*-diphenyl-4'-(5-(4'-(trifluoromethyl)-[1,1′-biphenyl]-4-yl)pyrazin-2-yl)-[1,1′-biphenyl]-4-amine (4d)**. Yield: 271 mg (81%); yellow powder, m.p: 306–308 °C. ^{1}H NMR (500 MHz, $CDCl_3$) δ 9.15 (s, 2H), 8.20 (d, $J = 8.1$ Hz, 2H), 8.16 (d, $J = 8.1$ Hz, 2H), 7.78 (d, $J = 8.2$ Hz, 4H), 7.75 (m, 4H), 7.56 (d, $J = 8.4$ Hz, 2H), 7.29 (t, $J = 7.8$ Hz, 4H), 7.16 (m, 6H), 7.06 (t, $J = 7.3$ Hz, 2H). ^{13}C NMR (126 MHz, $CDCl_3$) δ 150.61, 149.77, 147.79, 147.57, 143.87, 142.14, 141.23, 141.21, 140.96, 136.17, 134.48, 133.82, 129.56 (q, $J = 32.8$ Hz), 129.35, 127.94, 127.75, 127.42, 127.34, 127.19 **x** 2, 125.87 (q, $J = 3.8$ Hz), 124.66, 124.25 (q, $J = 272.0$ Hz), 123.63, 123.19. HRMS (ESI) *m/z*; $[M+H]^+$ Calcd for $C_{41}H_{28}F_3N_3$, 620.2309; found 620.2286.

***N,N*-diphenyl-4'-(5-(4'-(trifluoromethoxy)-[1,1′-biphenyl]-4-yl)pyrazin-2-yl)-[1,1′-biphenyl]-4-amine (4e)**. Yield: 312 mg (91%); yellow powder, m.p: 283–285 °C. ^{1}H NMR (500 MHz, $CDCl_3$) δ 9.14 (s, 2H), 8.18 (d, $J = 8.2$ Hz, 2H), 8.15 (d, $J = 8.2$ Hz, 2H), 7.74 (m, 4H), 7.68 (d, $J = 8.5$ Hz, 2H), 7.56 (d, $J = 8.4$ Hz, 2H), 7.33 (d, $J = 8.3$ Hz, 2H), 7.29 (t, $J = 7.8$ Hz, 4H), 7.16 (m, 6H), 7.06 (t, $J = 7.3$ Hz, 2H). ^{13}C NMR (126 MHz, $CDCl_3$) δ 150.49, 149.89, 149.02 (q, $J = 1.8$ Hz), 147.77, 147.57, 142.09, 141.19, 141.18, 141.08, 139.09, 135.65, 134.52, 133.83, 129.35, 128.49, 127.74 × 2, 127.27, 127.18 **x** 2, 124.65, 123.64, 123.19, 121.36, 120.54 (q, $J = 257.3$ Hz). HRMS (ESI) *m/z*; $[M+H]^+$ Calcd for $C_{41}H_{28}F_3N_3O$, 636.2258; found 636.2247.

4'-(5-(3′,5′-bis(trifluoromethyl)-[1,1′-biphenyl]-4-yl)pyrazin-2-yl)-*N,N*-diphenyl-[1,1′-biphenyl]-4-amine (4f). Yield: 310 mg (84%); canary yellow powder, m.p: 108–110 °C. ^{1}H NMR (500 MHz, $CDCl_3$) δ 9.15 (s, 2H), 8.24 (d, $J = 8.2$ Hz, 2H), 8.15 (d, $J = 8.2$ Hz, 2H), 8.09 (s, 2H), 7.90 (s, 1H), 7.79 (d, $J = 8.2$ Hz, 2H), 7.75 (d, $J = 8.2$ Hz, 2H), 7.56 (d, $J = 8.5$ Hz, 2H), 7.29 (t, $J = 7.8$ Hz, 4H), 7.16 (m, 6H), 7.06 (t, $J = 7.3$ Hz, 2H). ^{13}C NMR (126 MHz, $CDCl_3$) δ 150.82, 149.40, 147.80, 147.56, 142.50, 142.21, 141.26, 141.23, 139.30, 136.87, 134.38, 133.75, 132.33 (q, $J = 33.3$ Hz), 129.36, 127.91, 127.74, 127.57, 127.22, 127.19, 127.17 (q, $J = 2.8$ Hz), 124.66, 123.61, 123.35 (q, $J = 272.7$ Hz), 123.21, 121.32 (hept, $J = 3.4$ Hz). HRMS (ESI) *m/z*; $[M+H]^+$ Calcd for $C_{42}H_{27}F_6N_3$, 688.2182; found 688.2168.

4'-(5-(4'-(diphenylamino)-[1,1′-biphenyl]-4-yl)pyrazin-2-yl)-[1,1′-biphenyl]-4-carbonitrile (4g). Yield: 262 mg (84%); yellow powder, m.p: 296–298 °C. ^{1}H NMR (500 MHz, $CDCl_3$) δ 9.15 (s, 1H), 9.14 (s, 1H), 8.21 (d, $J = 8.3$ Hz, 2H), 8.15 (d, $J = 8.4$ Hz, 2H), 7.78–7.74 (m, 8H), 7.56 (d, $J = 8.6$ Hz, 2H), 7.29 (t, $J = 7.9$ Hz, 4H), 7.18–7.15 (m, 6H), 7.06 (t, $J = 7.3$ Hz, 2H). ^{13}C NMR (126 MHz, $CDCl_3$) δ 150.72, 149.54, 147.78, 147.54, 144.78, 142.18, 141.23 × 2, 140.29, 136.60, 134.39, 133.74, 132.73, 129.35, 127.90, 127.73, 127.72, 127.42, 127.19, 127.19, 124.65, 123.60, 123.19, 118.84, 111.37. HRMS (ESI) *m/z*; $[M+H]^+$ Calcd for $C_{41}H_{28}N_4$, 577.2387; found 577.2367.

4'-(5-(4′-nitro-[1,1′-biphenyl]-4-yl)pyrazin-2-yl)-*N,N*-diphenyl-[1,1′-biphenyl]-4-amine (4h). Yield: 216 mg (67%); red crystals, m.p: 277–279 °C. ^{1}H NMR (500 MHz, $CDCl_3$) δ 9.16 (s, 2H), 8.35 (d, $J = 8.6$ Hz, 2H), 8.23 (d, $J = 8.1$ Hz, 2H), 8.16 (d, $J = 8.1$ Hz, 2H), 7.82 (m, 4H), 7.76 (d, $J = 8.2$ Hz, 2H), 7.56 (d, $J = 8.4$ Hz, 2H), 7.29 (t, $J = 7.5$ Hz, 4H), 7.17 (m, 6H), 7.06 (t, $J = 7.3$ Hz, 2H). ^{13}C NMR (126 MHz, $CDCl_3$) δ 150.78, 149.46, 147.78, 147.52, 147.34, 146.72, 142.19, 141.26, 141.24, 139.87, 136.83, 134.36, 133.71, 129.35, 128.07, 127.82, 127.73, 127.44, 127.20, 127.19, 124.64, 124.26, 123.59, 123.19. HRMS (ESI) *m/z*; $[M+H]^+$ Calcd for $C_{40}H_{28}N_4O_2$, 597.2286; found 597.2258.

***N,N*-diphenyl-4'-(6-(4'-(trifluoromethyl)-[1,1′-biphenyl]-4-yl)pyrazin-2-yl)-[1,1′-biphenyl]-4-amine (8d).** Yield: 241 mg (72%); pale yellow powder, m.p: 83–85 °C. ^{1}H NMR (500 MHz, $CDCl_3$) δ 9.03 (s, 1H), 9.01 (s, 1H), 8.28 (d, $J = 8.2$ Hz, 2H), 8.23 (d, $J = 8.2$ Hz, 2H), 7.75 (m, 8H), 7.56 (d, $J = 8.4$ Hz, 2H), 7.29 (t, $J = 7.7$ Hz, 4H), 7.14–7.18 (m, 6H), 7.06 (t, $J = 7.3$ Hz, 2H). ^{13}C NMR (126 MHz, $CDCl_3$) δ 151.38, 150.89, 147.77, 147.54, 143.87, 142.25, 141.12, 140.03, 139.69, 136.38, 134.68, 133.80, 129.79 (q, $J = 32.7$ Hz), 129.35, 127.87, 127.75, 127.63, 127.43 **x** 2, 127.11, 125.87 (q, $J = 3.6$ Hz), 124.64, 124.24 (q, $J = 271.7$ Hz), 123.61, 123.19. HRMS (ESI) *m/z*; $[M+H]^+$ Calcd for $C_{41}H_{28}F_3N_3$, 620.2309; found 620.2289.

***N,N*-diphenyl-4'-(6-(4'-(trifluoromethoxy)-[1,1′-biphenyl]-4-yl)pyrazin-2-yl)-[1,1′-biphenyl]-4-amine (8e).** Yield: 254 mg (74%); pale yellow powder, m.p: 77–79 °C. ^{1}H NMR (500 MHz, $CDCl_3$) δ 9.01 (s, 1H), 9.00 (s, 1H), 8.26 (d, $J = 8.0$ Hz, 2H), 8.23 (d, $J = 8.1$ Hz, 2H), 7.74 (t, $J = 7.8$ Hz, 4H), 7.68 (d, $J = 8.3$ Hz, 2H), 7.55 (d, $J = 8.2$ Hz, 2H), 7.33 (d, $J = 8.1$ Hz, 2H), 7.29 (t, $J = 7.6$ Hz, 4H), 7.13–7.19 (m, 6H), 7.06 (t, $J = 7.2$ Hz, 2H). ^{13}C NMR (126 MHz, $CDCl_3$) δ 151.32, 150.97, 149.00 (q, $J = 1.6$ Hz), 147.75, 147.55, 142.20, 141.22, 139.91, 139.66, 139.10, 135.85, 134.72, 133.82, 129.35, 128.49, 127.74, 127.66, 127.56, 127.41, 127.10, 124.63, 123.61, 123.18, 121.37, 120.52 (q, $J = 257.3$ Hz). HRMS (ESI) *m/z*; $[M+H]^+$ Calcd for $C_{41}H_{28}F_3N_3O$, 636.2258; found 636.2240.

4'-(6-(3′,5′-bis(trifluoromethyl)-[1,1′-biphenyl]-4-yl)pyrazin-2-yl)-*N,N*-diphenyl-[1,1′-biphenyl]-4-amine (8f). Yield: 267 mg (72%); pale yellow powder, m.p: 190–192 °C. ^{1}H NMR (500 MHz, $CDCl_3$) δ 9.05 (s, 1H), 9.02 (s, 1H), 8.32 (d, $J = 8.4$ Hz, 2H), 8.24 (d, $J = 8.4$ Hz, 2H), 8.09 (s, 2H), 7.91 (s, 1H), 7.79 (d, $J = 8.4$ Hz, 2H), 7.76 (d, $J = 8.4$ Hz, 2H), 7.58–7.54 (m, 2H), 7.29 (dd, $J = 11.2$, 4.6 Hz, 4H), 7.19–7.14 (m, 6H), 7.06 (t, $J = 7.3$ Hz, 2H). ^{13}C NMR (126 MHz, $CDCl_3$) δ 151.47, 150.58, 147.80, 147.54, 142.53, 142.33, 140.27, 139.73, 139.50, 137.11, 134.60, 133.77, 132.32 (q, $J = 33.3$ Hz), 129.36, 127.89, 127.85, 127.76, 127.44, 127.20 (q, $J = 2.8$ Hz), 127.15, 124.66, 123.60, 123.34 (q, $J = 272.9$ Hz), 123.20, 121.35 (hept, $J = 3.5$ Hz). HRMS (ESI) *m/z*; $[M+H]^+$ Calcd for $C_{42}H_{27}F_6N_3$, 688.2182; found 688.2169.

4'-(6-(4'-(diphenylamino)-[1,1′-biphenyl]-4-yl)pyrazin-2-yl)-[1,1′-biphenyl]-4-carbonitrile (8g). Yield: 209 mg (67%); yellow powder, m.p: 115–116 °C. ^{1}H NMR (500 MHz, $CDCl_3$) δ 9.04 (s, 1H), 9.02 (s, 1H), 8.30 (d, $J = 8.3$ Hz, 2H), 8.23 (d, $J = 8.3$ Hz, 2H), 7.79–7.75 (m, 8H), 7.56 (d, $J = 8.6$ Hz, 2H), 7.29 (t, $J = 7.9$ Hz, 4H), 7.19–7.15 (m, 6H), 7.06 (t, $J = 7.3$ Hz, 2H). ^{13}C NMR (126 MHz, $CDCl_3$) δ 151.44, 150.70, 147.79, 147.54, 144.82, 142.30, 140.49, 140.18, 139.71, 136.84, 134.63, 133.76, 132.74, 129.36, 127.84, 127.75 × 3, 127.43, 127.13, 124.65, 123.59, 123.20, 118.84, 111.40. HRMS (ESI) *m/z*; $[M+H]^+$ Calcd for $C_{41}H_{28}N_4$, 577.2387; found 577.2377.

4'-(6-(4′-nitro-[1,1′-biphenyl]-4-yl)pyrazin-2-yl)-*N,N*-diphenyl-[1,1′-biphenyl]-4-amine (8h). Yield: 271 mg (84%); orange powder, m.p: 213–215 °C. ^{1}H NMR (500 MHz, $CDCl_3$) δ 9.05 (s, 1H), 9.03 (s, 1H), 8.35 (d, $J = 8.7$ Hz, 2H), 8.32 (d, $J = 8.3$ Hz, 2H), 8.24 (d, $J = 8.3$ Hz, 2H), 7.82 (m, 4H), 7.76 (d, $J = 8.3$ Hz, 2H), 7.56 (d, $J = 8.5$ Hz, 2H), 7.29 (t, $J = 7.8$ Hz, 4H), 7.14–7.19 (m, 6H), 7.06 (t, $J = 7.3$ Hz, 2H). ^{13}C NMR (126 MHz, $CDCl_3$) δ 151.48, 150.65, 147.82, 147.56, 147.40, 146.76, 142.34, 140.25, 140.09, 139.73, 137.11, 134.62, 133.77, 129.36, 128.01, 127.86,

127.78, 127.76, 127.44, 127.14, 124.67, 124.26, 123.60, 123.22. HRMS (ESI) *m/z*; $[M+H]^+$ Calcd for $C_{40}H_{28}N_4O_2$, 597.2286; found 597.2266.

Synthesis of chromophore 4i. 2,5-bis(4-bromophenyl)pyrazine (**2**) (300 mg, 0.77 mmol) was dissolved in dioxane (4 mL). Subsequently, $PdCl_2$(dppf) (58 mg, 10 mol%), CuI (15 mg, 10 mol%), 4-ethynyl-*N,N*-dimethylaniline (335 mg, 2.31 mmol) and TEA (1.07 mL, 7.7 mmol) were added to the reaction mixture and stirred at 100 °C for 1 h under MW. After cooling to RT, water was added and the mixture was extracted with CH_2Cl_2 (3 × 10 mL). The combined organic layer was washed with water and dried over anhydrous Na_2SO_4. The solvent was evaporated in vacuum, and the crude product was purified by silica column chromatography (CH_2Cl_2: MeOH, 10:1, v/v) to afford the desired compound **4i**. Similarly, compound **8i** was obtained using 2,6-bis(4-bromophenyl)pyrazine.

4,4'-((pyrazine-2,5-diylbis(4,1-phenylene))bis(ethyne-2,1-diyl))bis(*N,N*-dimethylaniline) (4i). Yield: 228 mg (57%); light brown powder, m.p: 344–345 °C. ^{1}H NMR (500 MHz, $CDCl_3$) δ 9.09 (s, 2H), 8.06 (d, J = 8.3 Hz, 4H), 7.65 (d, J = 8.4 Hz, 4H), 7.45 (d, J = 8.5 Hz, 4H), 6.68 (d, J = 8.7 Hz, 4H), 3.01 (s, 12H). HRMS (ESI) *m/z*; $[M+H]^+$ Calcd for 519.2543, found 519.2531.

4,4'-((pyrazine-2,6-diylbis(4,1-phenylene))bis(ethyne-2,1-diyl))bis(*N,N*-dimethylaniline) (8i). Yield: 192 mg (48%); yellow powder, m.p: 269–271 °C. ^{1}H NMR (500 MHz, $CDCl_3$) δ 8.97 (s, 2H), 8.15 (d, J = 8.3 Hz, 4H), 7.66 (d, J = 8.3 Hz, 4H), 7.45 (d, J = 8.8 Hz, 4H), 6.68 (d, J = 8.8 Hz, 4H), 3.01 (s, 12H). ^{13}C NMR (126 MHz, $CDCl_3$) δ 150.96, 150.28, 139.80, 135.12, 132.88, 131.82, 126.80, 125.90, 111.83, 109.69, 92.92, 87.28, 40.21. HRMS (ESI) *m/z*; $[M+H]^+$ Calcd for $C_{36}H_{30}N_4$, 519.2543; found 519.2535.

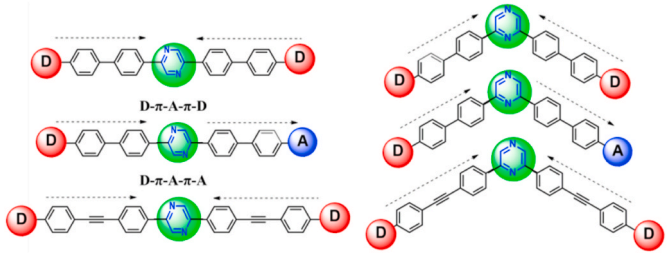

Fig. 1. Conjugation pathway in linear and angular chromophores.

3. Results and discussion

3.1. Synthesis

The detailed synthetic routes for linear and angular pyrazine derivatives are outlined in Schemes 1 and 2. The preparation of target chromophores having various D-A groups was accomplished by the typical Suzuki reaction with satisfactory yields [40]. Boronic acids functionalized with different donor (NMe_2, NPh_2, and carbazole) and acceptor groups (CF_3, OCF_3, CN, and NO_2) were used. In the structural design, we chose bis(4-bromophenyl)pyrazine (**2,6**) as a starting material [41,42], which is prepared by using dibromopyrazine (**1,5**) and (4-bromophenyl)boronic acid as a coupling partners. Attempts to prepare mono-substituted compounds **3,7** by utilizing bis(4-bromophenyl) pyrazine yielded a mixture of mono and disubstituted products, which were separated by column chromatography.

Symmetric linear and bent chromophores **4(b-c)** and **8(a-c)** were obtained by $Pd(PPh_3)_4$ catalysed Suzuki cross-coupling reaction of precursor **2,6** with two equivalents of appropriate boronic acid under microwave (MW) condition. Next, monosubstituted derivatives **3,7** were used as coupling partners to construct asymmetrical chromophores **4(d-h)** and **8(d-h)** with satisfactory yields. The compounds **4i** and **8i** with the π-linker separated from the acceptor by an additional triple bond were obtained via Sonogashira cross-coupling reaction of the bis(4-bromophenyl)pyrazine (**2,6**) with 4-ethynyl-*N,N*-dimethylaniline under MW with moderate yields [43]. The final products have been carefully purified by column chromatography and characterized by standard spectroscopic methods. The synthesized compounds are soluble in solvents such as chloroform, dichloromethane, acetone, and THF.

3.2. Photophysical properties

The optical properties of both linear **4(b-i)** and bent shaped **8(a-i)** chromophores were studied by absorption and photoluminescence (PL) spectra in CH_2Cl_2 solution. To estimate the molar extinction coefficients in CH_2Cl_2, the Lambert-Beer law was verified in 10^{-5} M concentration. The representative absorption spectra of selected chromophores are shown in Fig. 2 (SI data) and the results are summarized in Table 1. The absorption spectra of both linear and bent chromophores exhibited two distinct absorption bands in the range of 240–316 nm and 343–390 nm,

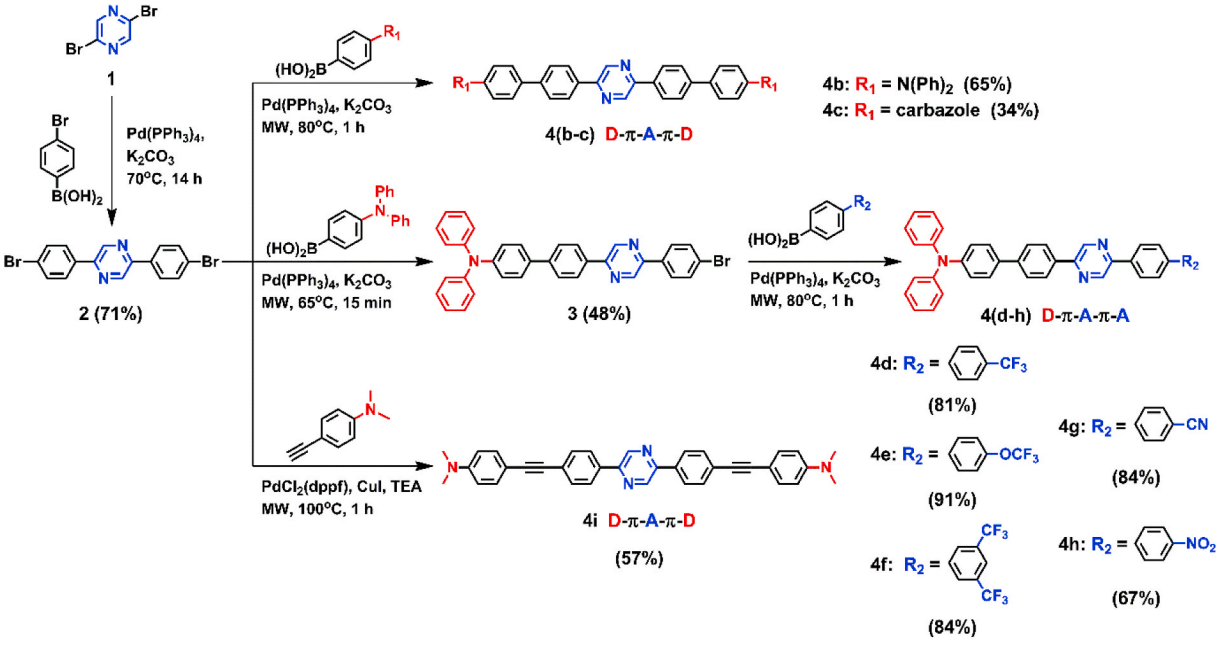

Scheme 1. Synthesis of linear chromophores **4(b-i).**

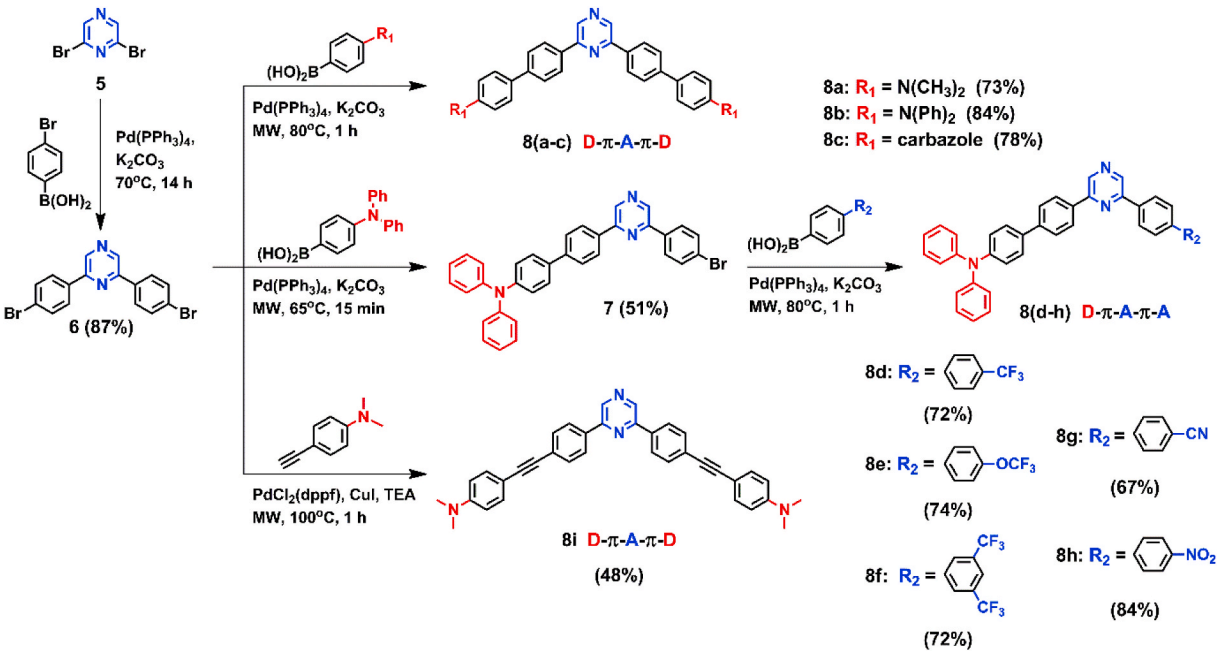

Scheme 2. Synthetic route for bent shaped chromophores **8(a-i)**.

Table 1
Summary of the optical, electrochemical, and thermal properties of compounds.

Cpd	λ_{abs} (nm)[a]	ε (mM^{-1} cm^{-1})[a]	PL (nm)[b] Soln	PL (nm)[b] Solid	Stokes shift (cm^{-1})	Φ_F[c]	E_{ox} (V)	HOMO (eV)[d]	LUMO (eVe[f]	T_d (°C)[f]
4b	301, 388	50.0	527	480	6798	0.21	0.80	−5.20	−2.38	508
4c	293, 358	42.4	466	–	6474	0.42	0.90	−5.30	−2.19	483
4d	307, 377	24.5	545	534	8177	0.3	0.94	−5.34	−2.46	431
4e	307, 375	35.6	538	519	8079	0.29	0.91	−5.31	−2.42	435
4f	308, 381	25.0	551	500	8098	0.31	0.93	−5.33	−2.47	446
4g	309, 379	22.2	558	545	8464	0.26	0.94	−5.33	−2.47	451
4h	316, 381	40.5	–	–	–	0.17	0.88	−5.28	−2.45	372
4i	300, 397	39.9	562	573	7395	0.19	0.82	−5.22	−2.49	–
8a	240, 370	40.4	524	486	7943	0.31	0.90	−5.30	−2.34	421
8b	298, 368	42.5	500	495	7174	0.49	0.79	−5.19	−2.21	512
8c	293, 343	45.8	441	–	6479	0.24	0.92	−5.32	−2.05	518
8d	295, 363	38.5	507	470	7824	0.31	0.75	−5.15	−2.15	435
8e	295, 363	36.2	505	495	7746	0.22	0.81	−5.21	−2.20	457
8f	292, 364	23.9	517	473	8130	0.19	0.83	−5.23	−2.24	445
8g	298, 363	33.5	518	517	8243	0.16	0.84	−5.24	−2.24	442
8h	307, 360	34.8	–	–	–	0.21	0.81	−5.21	−2.20	396
8i	290, 380	52.9	527	493	7340	0.42	0.87	−5.27	−2.36	322

[e] $LUMO = HOMO + E_g^{opt}$.
[a] Maximum absorption wavelength in CH_2Cl_2. ε: molar absorption coefficient.
[b] Maximum emission wavelength, soln: CH_2Cl_2, solid: powder.
[c] Fluorescence quantum yield determined relative to Rhodamine 6G.
[d] Electrochemical method was used to obtain the HOMO energy estimated from onset voltage of the first oxidation potential. HOMO = -(E_{ox}+4.4).
[f] T_d observed from TGA loss at 10 °C min^{-1} under nitrogen.

respectively. The shorter one is attributed to π-π* transition, while the other band corresponds to the charge-transfer interactions. Chromophore **4b** exhibits prominent red-shift in both absorption and emission bands with respect to **4c,** due to strong D-A interaction, as triphenylamine is strong electron-donating group compared to 9H-carbazole [44]. Among D-π-A-π-A compounds, **4g** displays large bathochromic shift (558 nm), due to increase in conjugation length. To gain insight into the molecular geometry, we compared the absorption spectra of linear and angular compounds. It was observed that angular chromophores showed hypsochromic shift compared to their linear counterparts. As we have anticipated, introducing D and/or A groups to the pyrazine derivatives prominently helps to red-shift the absorption spectra. However, biphenylene linker decreases the absorption maximum wavelength, but increases the emission maximum wavelength [38,45] (see Table 2).

The emission spectra of pyrazine-based compounds show nice tuning of emission wavelength ranging from 441 to 573 nm (Fig. 2 and SI data). All compounds are colored and strongly fluorescent in both solid and solution state (Fig. 3) except for nitro derivatives (**4h** and **8h**). Linear chromophores exhibited emission maxima in the relatively longer-wavelength region than those of the bent shaped molecules. The most red-shifted emission profile was observed for **4g** and **8g**, due to the presence of strong electron-withdrawing group (CN). The target compounds showed large Stokes shift (6474-8464 cm^{-1}), with fluorescence quantum yield between 0.16 and 0.49. The large Stokes shift observed for these pyrazine derivatives is based on the large energy difference between the excited and ground state of the molecules. The emission quenching of nitro derivatives **4h** and **8h** were relatively weak, due to

Table 2
Spectroscopic properties of the chromophores in different aprotic solvents.

Solvent	$E_T(30)$[a]	4b		8b		4g		8g	
		λ_{abs} (nm)	λ_{em} (nm)	λ_{abs} (nm)	λ_{em} (nm)	λ_{abs} (nm)	λ_{em} (nm)	λ_{abs} (nm)	λ_{em} (nm)
Hexane	30.9	383	430	367	408	382	435	357	414
Toluene	33.9	390	456	371	433	385	474	367	441
Dioxane	36.0	388	465	368	443	380	484	362	458
THF	37.4	391	503	369	474	383	534	363	481
CH_2Cl_2	41.1	388	527	370	500	379	558	363	518
Acetone	42.2	384	547	368	514	374	578	359	527
DMF	43.8	390	566	372	537	380	602	364	522

[a] E_T (30) Reichardt polarity parameter in kcal mol^{-1} [47].

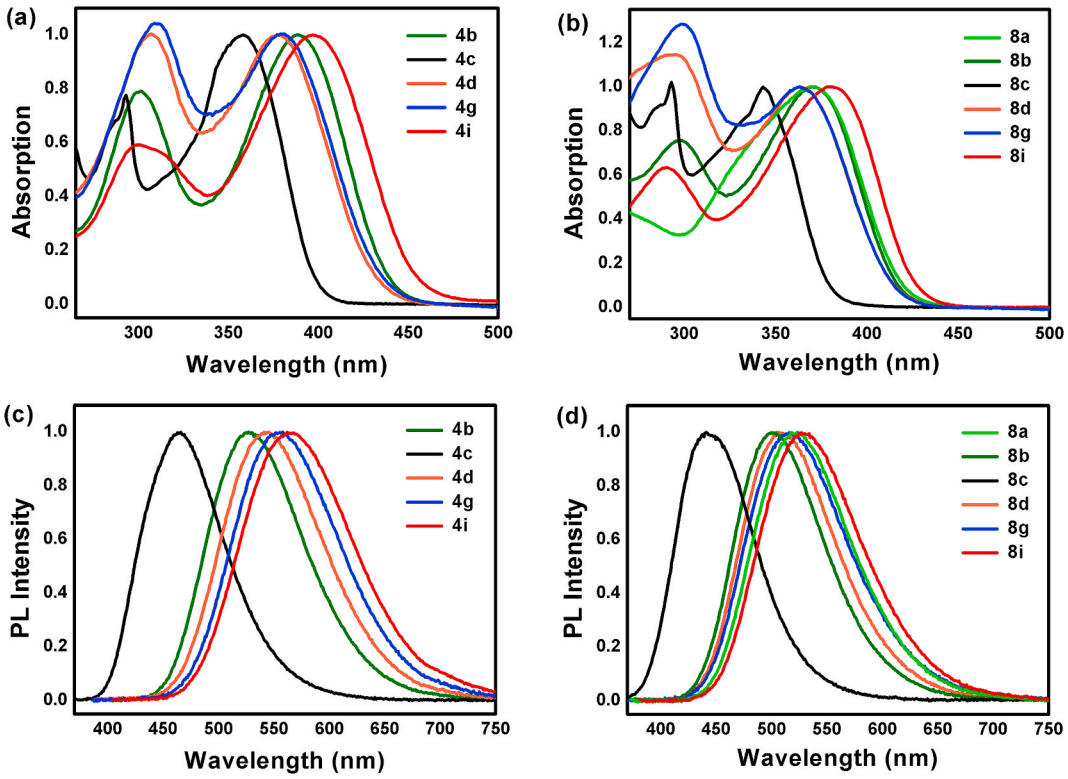

Fig. 2. (a–b) Normalized absorption spectra of linear and angular chromophores in CH_2Cl_2 solution. (c–d) Emission spectra of chromophores in CH_2Cl_2 (10^{-5} M) when excited at their absorption maxima.

efficient intersystem crossing [46]. The additional triple bond in compounds **4i** and **8i** led to red-shift of both absorption and emission spectra.

3.3. Solvatochromic effect

To study the solvatochromic properties of chromophores, we investigated the absorption and emission behavior of compounds in different solvents with varying polarity index (hexane, toluene, dioxane, THF, CH_2Cl_2, acetone, and DMF). Both linear (**4b**, **4g**) and bent (**8b**, **8g**) chromophores exhibited similar optical spectra that evidenced positive solvatochromic shifts. The slight red-shift on increasing the polarity solvent indicates ICT from the D to A group in the ground state (SI data), whereas it has a profound effect on the fluorescence spectra. The results show that the molecule is more solvated in the excited state.

The emission profiles of chromophores **4b** and **8b** showed a pronounced bathochromic shift of the emission band with increasing solvent polarity from hexane to DMF, reflecting the larger charge separation and higher dipole moment in the excited state than in the ground state. Solvent-polarity-dependent emission spectra are illustrates Fig. 4. The solvent dependence of emission spectra was further evaluated by the Dimroth-Reichardt $E_T(30)$ plot, which shows a good linear correlation. The emission maxima plotted against $E_T(30)$ showed linear plots for all tested solvents as shown in Fig. 5. When comparing different pyrazine derivatives, **8b** exhibited the highest regression line slopes (R^2 = 0.983).

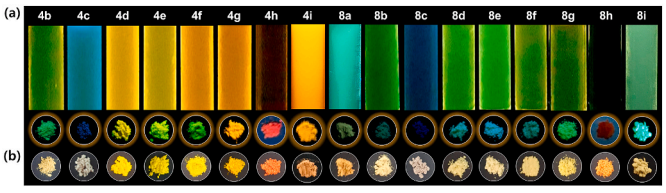

Fig. 3. Photographs of pyrazine derivatives (a) solution and solids samples under 365 nm UV light, and (b) solids under ambient light.

3.4. Acidochromism

In view of the importance of the acid-sensitive materials in the sensor industry, protonation studies of pyrazine derivatives (**4b** and **8b**) were

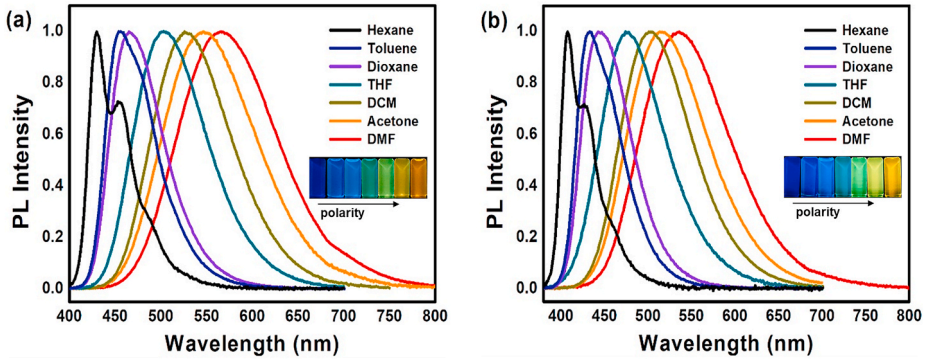

Fig. 4. Solvent-polarity-dependent emission spectra of (a) **4b** and (b) **8b** recorded in different solvents (10^{-5} M), the solutions were excited at their absorption maxima. Inset: Photographs of **4b** and **8b** taken under 365 nm UV light in different solvents.

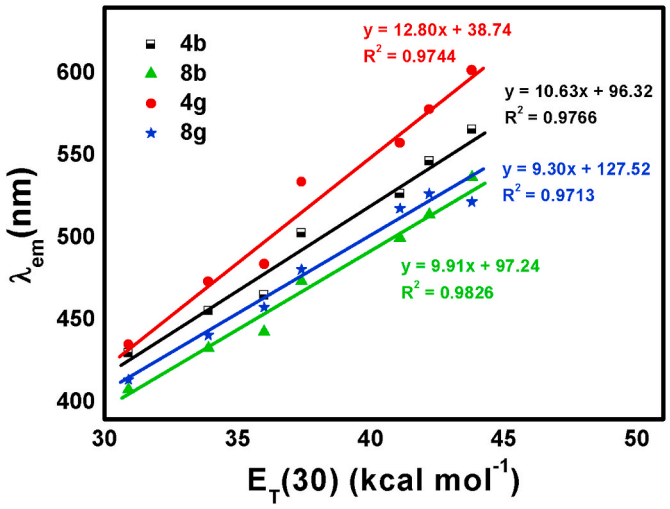

Fig. 5. Emission spectra of pyrazine derivatives as a function of the Dimroth-Reichardt polarity parameter.

undertaken. The absorption profile of compounds **4b** and **8b** on the incremental addition of trifluoroacetic acid (TFA) is illustrated in Fig. 6. As the concentration of TFA is increased, the peaks at 301 and 388 nm gradually decrease, and a new peak at 512 nm grows in **4b**. Similarly, in the case of **8b** peaks at 298 and 368 nm decrease, and new peaks starts to appear around 500 nm. The addition of excess TFA produces prominent red-shift, as protonation by TFA disrupts the electron-donating capability of nitrogen atom for charge transfer (CT) [48,49]. The observed isosbestic points suggests the presence of neutral and protonated species in equilibrium [50]. Finally, the addition of triethylamine (TEA) to fully protonated **4b** returns the original absorption spectrum. The emission spectra of chromophores **4b** and **8b** exhibited a sharp decrease in the intensity on the addition of TFA (Fig. 6) [51,52]. The protonated species experiences a more pronounced dipolar relaxation from the excited state due to the presence of strong D-A interactions. We have also investigated the sensitivity of compound **8a** towards acid-base by NMR measurements. The molecule **8a** in $CDCl_3$ exhibits its characteristic NMR signals. With the gradual addition of TFA, aromatic protons close to aromatic amine results in downfield shift from 6.7 ppm to 7.3 ppm (Fig. 7). These changes could be ascribed to the protonation by TFA, which increases the D-A interaction [53].

3.5. Aggregation-induced emission properties

The target pyrazine derivatives are highly fluorescent in both solution and aggregated state. Our speculation on the mechanism of enhanced emission is supported by the experimental absorption and PL data. DMF and water were used as the solvent pair because of good miscibility. The AIE characteristics of four selected luminogens (**4b**, **8b**, **4g**, and **8g**) with strong electron-donor (diphenylamine) and acceptor (CN) group were investigated through their fluorescent behaviour (Fig. 8 and SI data). These four compounds can be divided into two categories: **4b**, **8b**, and **4g** showed ICT plus aggregation enhanced emission (AEE) behavior while **8g** showed typical AIE behavior. At lower water percentage (f_w:<40%), the fluorescence spectra of compounds **4b**, **8b**, and **4g** show sudden decrease in fluorescence intensity, which is attributed to the solvent polarity dependent ICT emission. At higher water percentage (f_w: >40%), the emission spectra of pyrazine derivatives **4b**, **8b**, and **4g** show blue-shifted emission (567–609 nm to 471–545 nm) with enhanced intensity, and then gradually decreases. In the aggregated form, molecular rotation ceases, and leads to enhanced emission. The decrease in intensity is caused by the precipitation of nanoaggregates as the water percentage (f_w = 60–90%) increases, since the compounds are insoluble in water. Compound **8g** dissolved in pure DMF solution is virtually non-luminescent, but exhibits outstanding fluorescent enhancement for f_w > 50% and emits blue fluorescence. However, further addition of water to 99%, results in an obvious lowering of the emission intensity, due to decreased solubility (Fig. 8b) [54]. The AIE study clearly indicates the solvent polarity and AIE dependent emission behavior of these luminogens. The emission intensity of pyrazine-based compounds as a function of water volume fraction is shown in Fig. 9.

3.6. Thermal properties

Thermal stability is one of the key requirements for the practical applications of organic chromophores. The thermal properties of selected compounds were investigated by thermogravimetric analysis (TGA) and differential scanning calorimetry (DSC), which was carried out under a N_2 atmosphere at a heating rate of 10 °C/min. TGA curves reveals that all the materials exhibited high degradation temperatures (T_d corresponding to 5% weight loss) in the range 322–510 °C, which indicates that these chromophores are stable enough to fabricate into devices (Fig. 10 and SI data). The T_d values increased with the increasing size of the linkers [38]. Pyrazine derivatives showed single endothermic peak (SI data), presumably attributable to melting, at 331, 279, 325, and 215 °C on heating **4c**, **4h**, **8c**, and **8h**, respectively. The excellent thermal stability makes these pyrazine derivatives suitable for the potential device applications.

3.7. Electrochemical properties

The electron donor strengths of linear and angular pyrazine-based chromophores **4(b-i)** and **8(a-i)** were studied by cyclic voltammetry (CV) measurements in 0.1 M solution of $TBAPF_6$. Cyclic voltammograms

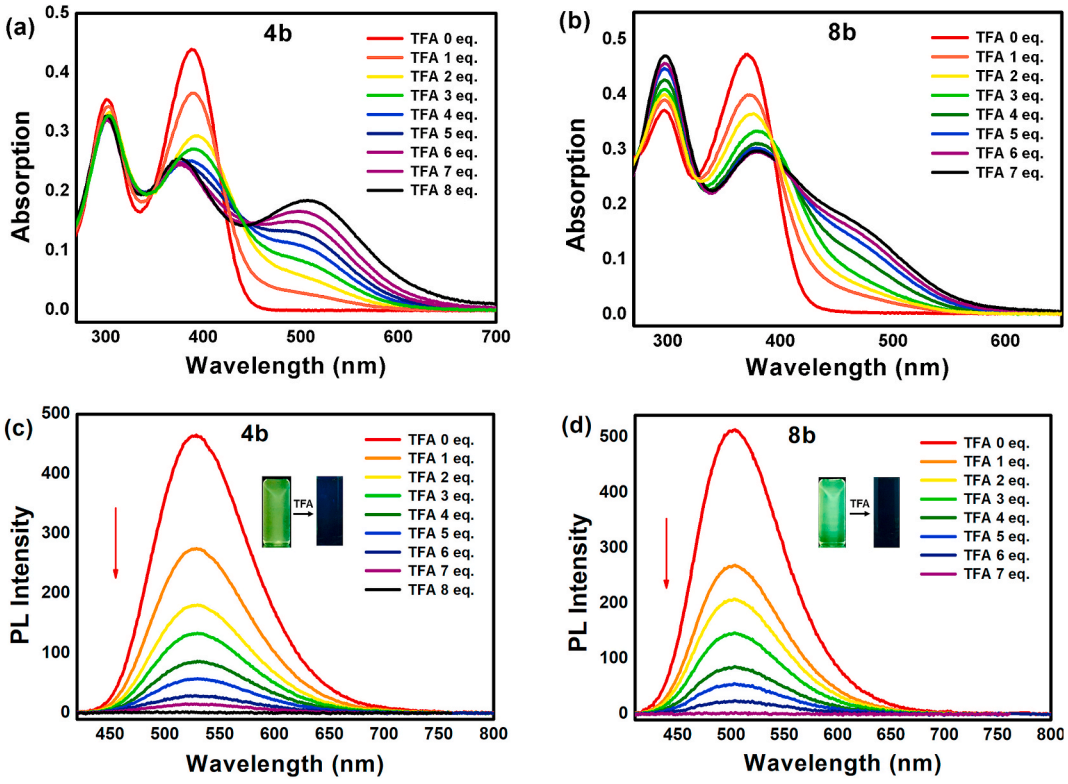

Fig. 6. (a–b) Absorption spectra, and (c–d) Emission spectra of compounds **4b** and **8b** in CH_2Cl_2 (10^{-5} M) with the gradual addition of TFA. Inset: photos of compounds before and after the addition of TFA under UV light (365 nm).

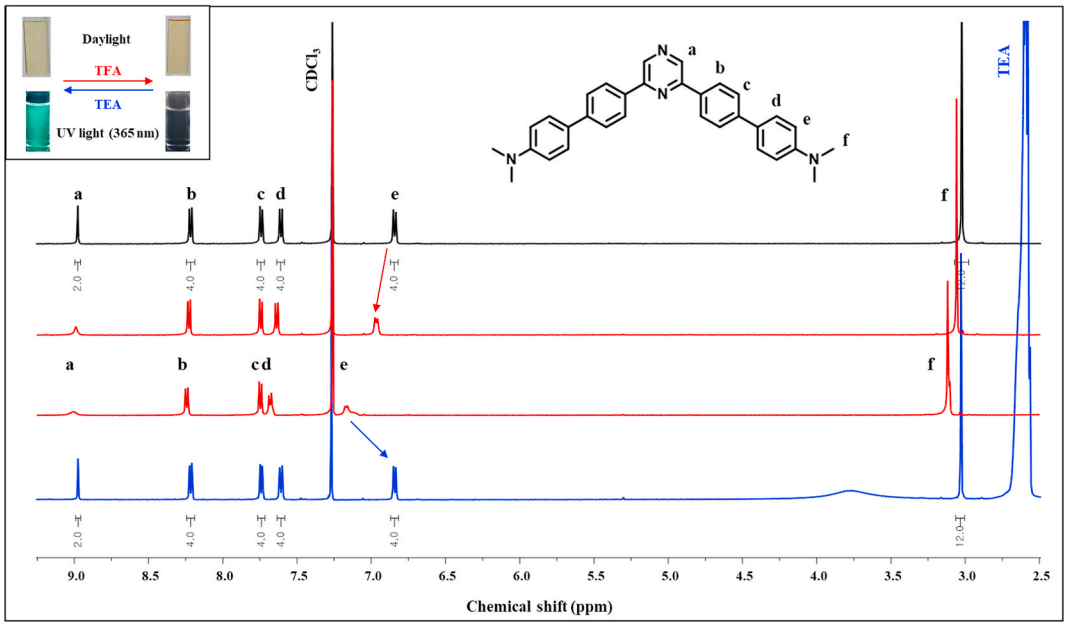

Fig. 7. ^{1}H NMR spectra of **8a** in $CDCl_3$ with addition of acid and base. The arrows highlight the shift.

of representative compounds are displayed in Fig. 11 (SI data) and the corresponding electrochemical data are summarized in Table 1. The highest occupied molecular orbital (HOMO) energy levels of all chromophores were calculated from first onset oxidation (E_{ox}) and lowest unoccupied molecular orbital (LUMO) energy levels were calculated using HOMO and the optical band gap (E_g^{opt}).

Both linear and bent shaped compounds **4(b-i)** and **8(a-i)** exhibited quasi-reversible oxidation waves and their oxidation potentials are in the range of 0.75–0.94 eV. The optical band gap compounds are in the range of 2.73–3.27 eV and the linear chromophores exhibit lower band gap (E_g) compared to bend shaped molecules. Chromophores **4c** and **8c** showed two well separated oxidation waves at 0.9 and 1.17 and 0.92 and 1.19 eV, respectively, due to oxidation of two carbazole moities [55]. In both linear and bent D-π-A-π-D series, *N,N*-diphenyl substituted chromophores (**4b**, **8b**) showed the lowest E_{ox} (0.79–0.80 eV), and in case of D-π-A-π-A, compounds **4h** and **8h** showed the lowest E_{ox}

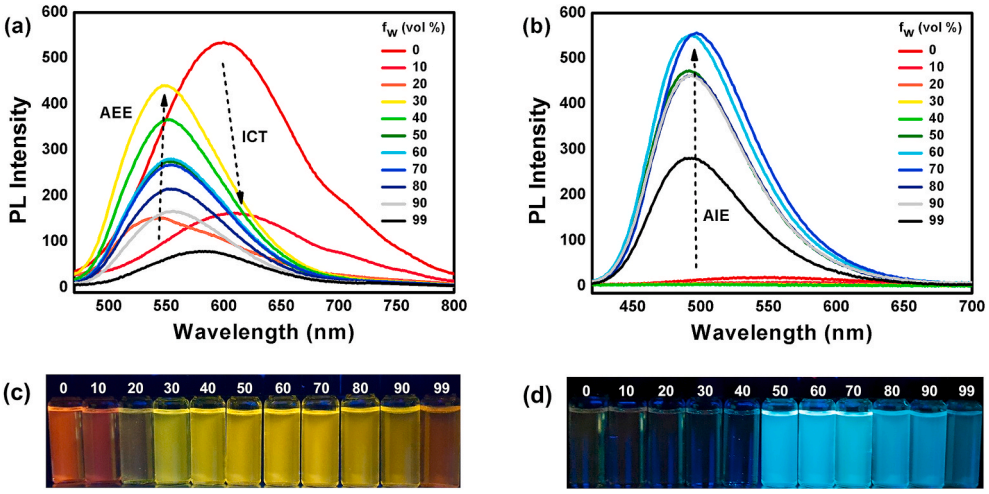

Fig. 8. Photoluminescence spectra of (a) **4g** and (b) **8g** in DMF/H_2O mixture with different water fractions (f_w). Photos of (c) **4g** and (d) **8g** in DMF/water mixtures taken under 365 nm UV light.

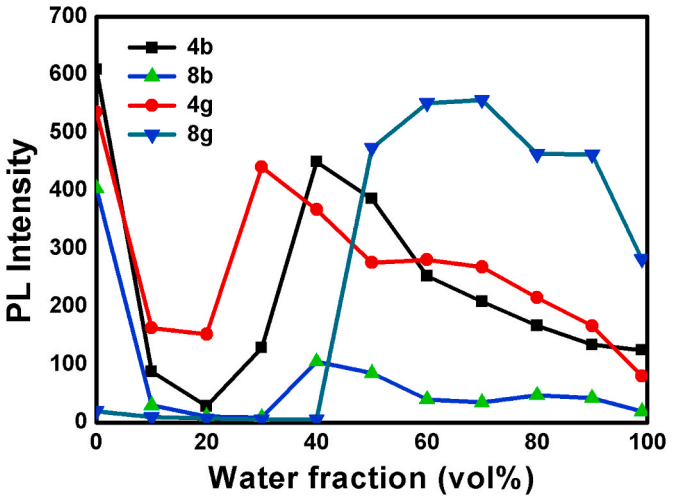

Fig. 9. Variation in the PL intensity of pyrazine derivatives in DMF/water mixtures (c = 10^{-5} M).

(0.81–0.88 eV). The cyclic voltammograms show that upon increasing the number of phenylenes, the first oxidation potential and optical band gap increase [38]. These results suggest that the orientation of the molecule and the end-capped donor acceptor groups significantly affect the electrochemical properties of the target chromophores.

3.8. Computational modeling

In order to understand the structural and electronic properties of linear and angular push-pull chromophores, density functional theory (DFT) calculations were carried out by employing the B3LYP/6-31G level of theory. The quantum-mechanical calculations were carried out using the Gaussian 09 package. The contours of the HOMO and LUMO are illustrated for selected compounds in Fig. 12 (SI data). The HOMO-LUMO energy gap, dipole moment (μ), and first-order hyperpolarizability (β) of the chromophores are listed in Table 3. The molecular orbitals of the compounds show different HOMO and LUMO energy levels, depending on their molecular structure. The static dipole moment and first-order hyperpolarizability were calculated by the following equations [56–58].

$$\mu_{tot} = (\mu_{\mathscr{X}}^2 + \mu_{\mathscr{Y}}^2 + \mu_{\mathscr{Z}}^2)^{1/2}$$

$$\beta_{tot} = [(\beta xxx + \beta xyy + \beta xzz)^2 + (\beta yyy + \beta yzz + \beta yxx)^2 + (\beta zzz + \beta zxx + \beta zyy)^2]^{1/2}$$

Where βxxx, βxyy, βxzz, βyyy, βyzz, βyxx, βzzz, βzxx, and βzyy are the tensor components.

In D-π-A-π-D compounds, the HOMO was localized on pyrazine and spread over donor groups (NMe_2, NPh_2 and carbazole), whereas the LUMO was localized mainly on pyrazine and π-linker. The HOMOs of D-π-A-π-A compounds is localized on the donor and the LUMO was completely localized on the pyrazine and the acceptor (CF_3, OCF_3, CN and NO_2), because of the strong electron-withdrawing nature. The electron density is transferred from the donor to the acceptor through the pyrazine and π-conjugated spacer acting as an electron relay. The calculated HOMO and LUMO energy levels range from −5.36/-4.85 and

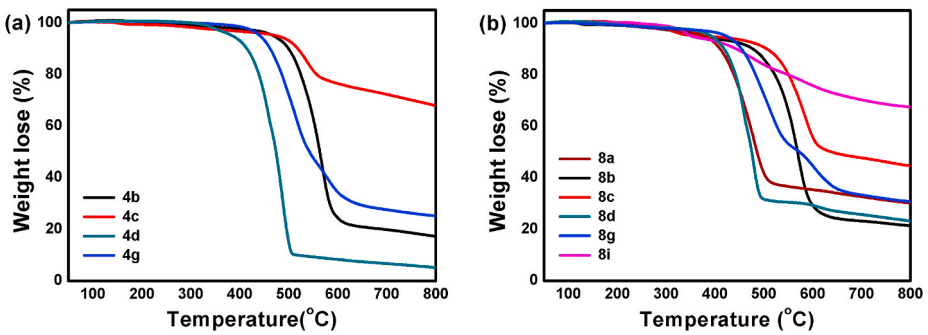

Fig. 10. TGA curves of representative (a) linear and (b) bent compounds determined at a heating rate of 10 °C min^{-1} under nitrogen atmosphere.

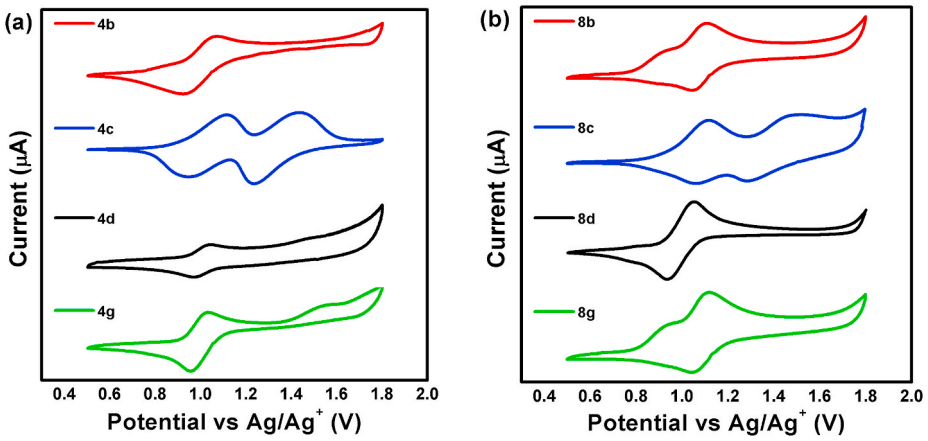

Fig. 11. Cyclic voltammograms of (a) linear and (b) bent compounds in CH_2Cl_2 with 0.1 M $TBAPF_6$ at a scan rate of 100 mV/s.

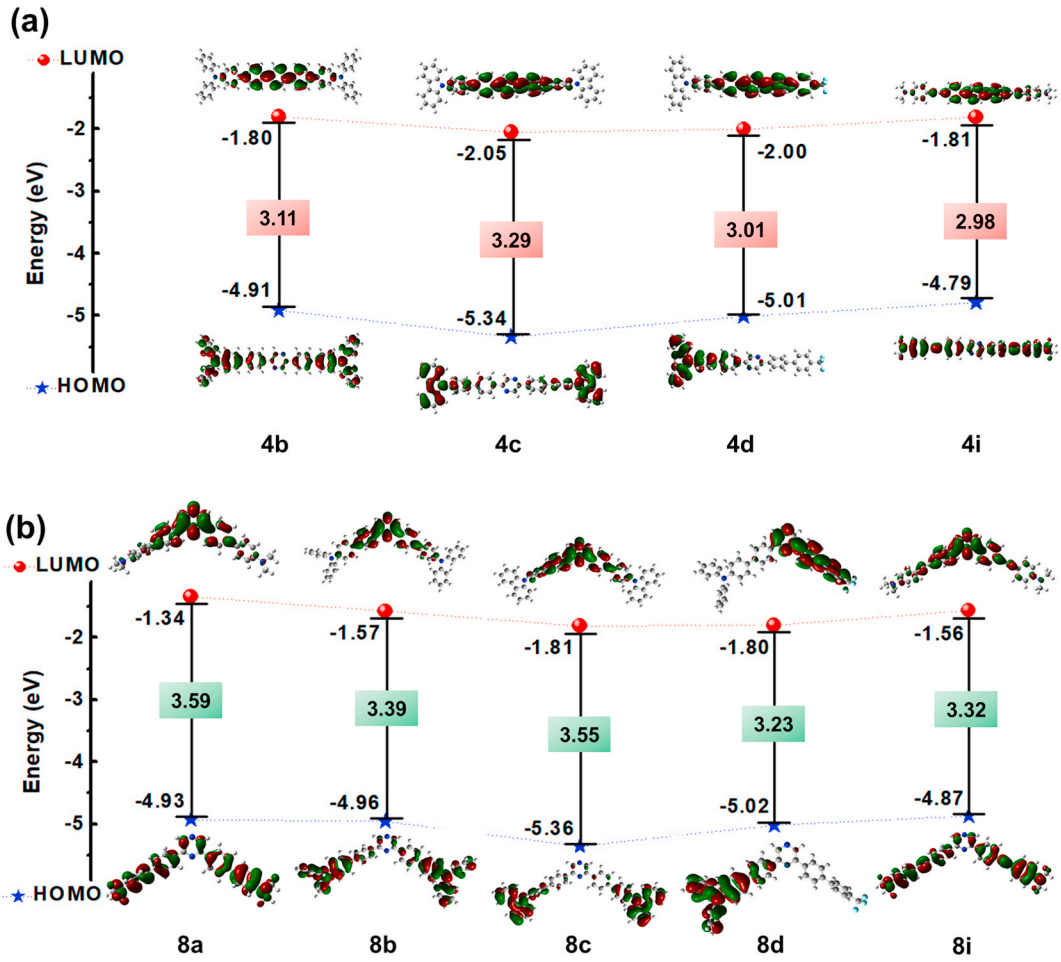

Fig. 12. Optimized molecular orbital amplitude plots of HOMO and LUMO energy levels, (a) linear and (b) bent shaped compounds calculated using the B3LYP/6-31G basis set.

−2.53/-1.34 eV, respectively. In linear compounds, stabilization of the LUMO energy level is more pronounced compared to HOMO, which results in decreased HOMO-LUMO gap. The calculated dipole moments of the chromophores range from 0.02 to 7.38 D. Molecules with D-π-A-π-D configuration exhibited lowest dipole moment. Chromophores **4h** and **8h** with strong electron acceptor (NO_2) resulted in a large dipole moment. The results suggest that modifications of the electron donating and accepting groups significantly influence the electronic structure of these compounds, which may tune their photophysical properties.

4. Conclusions

In summary, a series of pyrazine-based linear and bent structural isomers with D-π-A-π-D and D-π-A-π-A configurations were synthesized by the Suzuki cross-coupling reactions. Their optical, electrochemical and computational properties were explored, which show strong

Table 3
Calculated HOMO-LUMO energy levels for linear and bent shaped compounds.

Compound	HOMO (eV)[a]	LUMO (eV)[a]	E_g (eV)[a]	μ (D)[b]	E_g^{opt} (eV)[c]
4b	−4.91	−1.80	3.11	0.02	2.82
4c	−5.34	−2.05	3.29	0.05	3.11
4d	−5.01	−2.00	3.01	4.49	2.88
4e	−5.00	−1.96	3.04	3.94	2.89
4f	−5.03	−2.10	2.93	4.98	2.86
4g	−5.03	−2.16	2.87	6.99	2.86
4h	−5.04	−2.53	2.51	7.38	2.83
4i	−4.79	−1.81	2.98	0.35	2.73
8a	−4.93	−1.34	3.59	4.47	2.96
8b	−4.96	−1.57	3.39	2.17	2.98
8c	−5.36	−1.81	3.55	0.5	3.27
8d	−5.02	−1.80	3.23	3.68	3.00
8e	−5.02	−1.75	3.27	3.48	3.01
8f	−5.04	−1.92	3.11	4.09	2.99
8g	−5.05	−2.02	3.03	5.92	3.00
8h	−5.05	−2.53	2.52	6.25	3.01
8i	−4.87	−1.56	3.32	5.54	2.91

[a] HOMO-LUMO and band gap from DFT calculation.
[b] μ is the total dipole moment.
[c] Estimated from the absorption spectra $E_g^{opt} = 1240/\lambda_{onest}$.

electronic communication. The emission behaviour of pyrazine derivatives in both solution and aggregate states were studied. The presence of electron-rich units NMe_2 (**4a**, **8a**) results in lowering of the band gap, which leads to a bathochromic shift of the absorption spectrum. In addition luminogens **4b** and **8b** exhibited remarkable solvatochromic and acidochromic properties with a wide range of wavelength. Due to the synergetic interaction of the D-A moieties, chromophore **8g** shows an enhanced ICT process, which considerably quenches its fluorescence in solution and makes it possible to evaluate its AIE properties. These compounds possess reversible multistimuli-responsive fluorochromic properties. Therefore, we believe that these pyrazine-based luminogens will enrich the family of AIEgens and find wide application in fluorescent polarity sensors, bioprobes etc.

Declaration of competing interest

The authors declare that they have no known competing financial interests or personal relationships that could have appeared to influence the work reported in this paper.

Acknowledgement

This research was supported by the Basic Science Research Program through the National Research Foundation of Korea (NRF), funded by the Ministry of Education (No.2016R1D1A1B04932654) in Korea.

Appendix A. Supplementary data

Supplementary data to this article can be found online at https://doi.org/10.1016/j.dyepig.2021.109320.

Author statement

Hyung-Ha Park: Most of bench work for synthesis of the final materials. Puttavva Meti: Conceptualization, Methodology, Data curation, Validation, Investigation, Resources, Data curation, Writing – original draft. Young-Dae Gong: Writing – review & editing, Visualization, Supervision, Project administration, Funding acquisition.

References

[1] Faisal M, Hong Y, Liu J, Yu Y, Lam JWY, Qin A, et al. Fabrication of fluorescent silica nanoparticles hybridized with AIE luminogens and exploration of their applications as nanobiosensors in intracellular imaging. Chem Eur J 2010;16(14):4266–72.
[2] Ding D, Li K, Liu B, Tang BZ. Bioprobes based on AIE fluorogens. Acc Chem Res 2013;46(11):2441–53.
[3] Zhao Z, Deng C, Chen S, Lam JWY, Qin W, Lu P, et al. Full emission color tuning in luminogens constructed from tetraphenylethene, benzo-2,1,3-thiadiazole and thiophene building blocks. Chem Commun 2011;47(31):8847–9.
[4] Ning Z, Tian H. Triarylamine: a promising core unit for efficient photovoltaic materials. Chem Commun 2009;37:5483–95.
[5] Dong Y, Lam JWY, Qin A, Liu J, Li Z, Tang BZ, et al. Aggregation-induced emissions of tetraphenylethene derivatives and their utilities as chemical vapor sensors and in organic light-emitting diodes. Appl Phys Lett 2007;91(1).
[6] Liu Y, Tang Y, Barashkov NN, Irgibaeva IS, Lam JWY, Hu R, et al. Fluorescent chemosensor for detection and quantitation of carbon dioxide gas. J Am Chem Soc 2010;132(40):13951–3.
[7] Andrew TL, Swager TM. A fluorescence turn-on mechanism to detect high explosives RDX and PETN. J Am Chem Soc 2007;129(23):7254–5.
[8] Sun H, Tang X-X, Miao B-X, Yang Y, Ni Z. A new AIE and TICT-active tetraphenylethene-based thiazole compound: synthesis, structure, photophysical properties and application for water detection in organic solvents. Sensor Actuator B Chem 2018;267:448–56.
[9] Hong Y, Lam JWY, Tang BZ. Aggregation-induced emission. Chem Soc Rev 2011;40(11):5361–88.
[10] Thomas SW, Joly GD, Swager TM. Chemical sensors based on amplifying fluorescent conjugated polymers. Chem Rev 2007;107(4):1339–86.
[11] Zhang Z, Zhao Y, Zhang R, Zhang L, Cheng W, Ni ZH. Design and synthesis of a new series of tetra(polycyclic aryl)ethenes: achieving aggregation-induced emission and efficient solid-state photoluminescence. Dyes Pigments 2015;118:95–101.
[12] Kim TD, Lee KS. D-pi-A conjugated molecules for optoelectronic applications. Macromol Rapid Commun 2015;36(11):943–58.
[13] Mei J, Leung NL, Kwok RT, Lam JW, Tang BZ. Aggregation-induced emission: together we shine, united we soar! Chem Rev 2015;115(21):11718–940.
[14] Luo J, Xie Z, Lam JW, Cheng L, Chen H, Qiu C, et al. Aggregation-induced emission of 1-methyl-1,2,3,4,5-pentaphenylsilole. Chem Commun 2001;(18):1740–1.
[15] Zhang J, Chen R, Zhu Z, Adachi C, Zhang X, Lee C-S. Highly stable near-infrared fluorescent organic nanoparticles with a large Stokes shift for noninvasive long-term cellular imaging. ACS ACS Appl Mater Interfaces 2015;7(47):26266–74.
[16] Fischer I, Petkau-Milroy K, Dorland YL, Schenning APHJ, Brunsveld L. Self-assembled fluorescent organic nanoparticles for live-cell imaging. Chem Eur J 2013;19(49):16646–50.
[17] Yu J, Zhang X, Hao X, Zhang X, Zhou M, Lee CS, et al. Near-infrared fluorescence imaging using organic dye nanoparticles. Biomaterials 2014;35(10):3356–64.
[18] Mu G, Zhang W, Xu P, Wang H, Wang Y, Wang L, et al. Constructing new n-type, ambipolar, and p-type Aggregation-induced blue luminogens by gradually tuning the proportion of tetrahphenylethene and diphenylphophine oxide. *J Phys Chem* C 2014;118(16):8610–6.
[19] Shen XY, Wang YJ, Zhao E, Yuan WZ, Liu Y, Lu P, et al. Effects of substitution with donor-acceptor groups on the properties of tetraphenylethene trimer: aggregation-induced emission, solvatochromism, and mechanochromism. *J Phys Chem* C 2013;117(14):7334–47.
[20] Zhang X, Chi Z, Li H, Xu B, Li X, Liu S, et al. Synthesis and properties of novel aggregation-induced emission compounds with combined tetraphenylethylene and dicarbazolyl triphenylethylene moieties. J Mater Chem 2011;21(6):1788–96.
[21] Garzón A, Fernández-Liencres MP, Moral M, Peña-Ruiz T, Navarro A, Tolosa J, et al. Effect of the aggregation on the photophysical properties of a blue-emitting star-shaped molecule based on 1,3,5-tristyrylbenzene. *J Phys Chem* C 2017;121(8):4720–33.
[22] de Lera-Garrido F, Sánchez-Ruiz A, Rodríguez-López J, Tolosa J, García-Martínez JC. Enhancement of emission by surfactant-induced aggregation in poly(phenylenevinylene)-based lipochromophores. Dyes Pigments 2020;179:108410.
[23] Sánchez-Ruiz A, Rodríguez-López J, Garzón-Ruiz A, Jiménez-Pulido SB, Illán-Cabeza NA, Navarro A, et al. Shedding light on the origin of solid-state luminescence enhancement in butterfly molecules. Chem Eur J 2020;26(61):13990–4001.
[24] Zeng Q, Li Z, Dong Y, Di C, Qin A, Hong Y, et al. Fluorescence enhancements of benzene-cored luminophors by restricted intramolecular rotations: AIE and AIEE effects. Chem Commun 2007;(1):70–2.
[25] Hu R, Leung NLC, Tang BZ. AIE macromolecules: syntheses, structures and functionalities. Chem Soc Rev 2014;43(13):4494–562.
[26] Chen M, Li L, Wu H, Pan L, Li S, He B, et al. Unveiling the different emission behavior of polytriazoles constructed from pyrazine-based AIE monomers by click polymerization. ACS ACS Appl Mater Interfaces 2018;10(15):12181–8.
[27] Pan L, Cai Y, Wu H, Zhou F, Qin A, Wang Z, et al. Tetraphenylpyrazine-based luminogens with full-colour emission. Mater Chem Front 2018;2(7):1310–6.
[28] Chen M, Li L, Nie H, Tong J, Yan L, Xu B, et al. Tetraphenylpyrazine-based AIEgens: facile preparation and tunable light emission. Chem Sci 2015;6(3):1932–7.
[29] Qin A, Lam JWY, Mahtab F, Jim CKW, Tang L, Sun J, et al. Pyrazine luminogens with "free" and "locked" phenyl rings: understanding of restriction of intramolecular rotation as a cause for aggregation-induced emission. Appl Phys Lett 2009;94(25):253308.
[30] Song X, Kong L, Du H, Li X, Feng H, Zhao J, et al. Effects of pyrazine derivatives and substituted positions on the photoelectric properties and electromemory performance of D-A-D series compounds. Materials (Basel) 2018;11(10).
[31] Achelle S, Barsella A, Baudequin C, Caro B, Robin-le Guen F. Synthesis and photophysical investigation of a series of push-pull arylvinyldiazine chromophores. J Org Chem 2012;77(8):4087–96.
[32] Bureš F, Čermáková H, Kulhánek J, Ludwig M, Kuznik W, Kityk IV, et al. Structure-property relationships and nonlinear optical effects in donor-substituted

dicyanopyrazine-derived push-pull chromophores with enlarged and varied π-linkers. Eur J Org Chem 2012;3:529–38.
[33] Verbitskiy EV, Achelle S, Bureš F, le Poul P, Barsella A, Kvashnin YA, et al. Synthesis, photophysical and nonlinear optical properties of [1,2,5]oxadiazolo [3,4-b]pyrazine-based linear push-pull systems. J Photochem Photobiol Chem 2021;404:112900.
[34] Hoffert K, Durand RJ, Gauthier S, Robin-le Guen F, Achelle S. Synthesis and photophysical properties of a series of pyrazine-based push–pull chromophores. Eur J Org Chem 2017;3:523–9.
[35] Data P, Pander P, Okazaki M, Takeda Y, Minakata S, Monkman AP. Dibenzo[a,j] phenazine-Cored donor–acceptor–donor compounds as green-to-red/NIR thermally activated delayed fluorescence organic light emitters. Angew Chem Int Ed 2016;55(19):5739–44.
[36] Meti P, Park H-H, Gong Y-D. Recent developments in pyrazine functionalized π-conjugated materials for optoelectronic applications. J Mater Chem C 2020;8(2): 352–79.
[37] Kojima T, Nishida J-i, Tokito S, Tada H, Yamashita Y. Organic field-effect transistors based on heterocyclic co-oligomers containing a pyrazine ring. Chem Commun 2007;(14):1430–2.
[38] Park D-J, Meti P, Gong Y-D. Diarylpyrazine-based position isomers: a detailed study of optical properties and structure-property relationship. Dyes Pigments 2020;176:108254.
[39] Meti P, Park D-J, Gong Y-D. Structure property relationship of linear and angular pyrazine-based structural isomers with terminal D-A groups and evaluation of their photophysical properties. Dyes Pigments 2019;168:357–68.
[40] Almond-Thynne J, Blakemore DC, Pryde DC, Spivey AC. Site-selective Suzuki–Miyaura coupling of heteroaryl halides – understanding the trends for pharmaceutically important classes. Chem Sci 2017;8(1):40–62.
[41] Chen Z, Ye D, Xu G, Ye M, Liu L. Highly efficient synthesis of 2,5-disubstituted pyrazines from (Z)-β-haloenol acetates. Org Biomol Chem 2013;11(39):6699–702.
[42] Liu C, Zhao J, Qiao Y, Huang W, Rao Z, Gu Y. Selective synthesis of oxazoles and pyrazines from α-bromo-1-phenylethanone using a by-product-promoted strategy. Tetrahedron 2018;74(51):7351–7.
[43] Dokladalova L, Bures F, Kuznik W, Kityk IV, Wojciechowski A, Mikysek T, et al. Dicyanobenzene and dicyanopyrazine derived X-shaped charge-transfer chromophores: comparative and structure-property relationship study. Org Biomol Chem 2014;12(29):5517–27.
[44] Achelle S, Rodríguez-López J, Larbani M, Plaza-Pedroche R, Robin-le Guen F. Carbazole- and triphenylamine-substituted pyrimidines: synthesis and photophysical properties. Molecules 2019;24(9):1742.
[45] Achelle S, Robin-le Guen F. Emission properties of diazines chromophores: structure-properties relationship. J Photochem Photobiol Chem 2017;348:281–6.
[46] Collado-Fregoso E, Zugazagoitia JS, Plaza-Medina EF, Peon J. Excited-state dynamics of nitrated Push−Pull molecules: the importance of the relative energy of the singlet and triplet manifolds. J Phys Chem A 2009;113(48):13498–508.
[47] Reichardt C. Solvatochromic dyes as solvent polarity indicators. Chem Rev 1994;94 (8):2319–58.
[48] Meti P, Yang J-W, Gong Y-D. Structure property relationships of tunable donor-acceptor functionalized dipyrrolopyrazine derivative as selective reversible acid base sensor. Dyes Pigments 2018;156:233–42.
[49] Singh P, Baheti A, Thomas KR. Synthesis and optical properties of acidochromic amine-substituted benzo[a]phenazines. J Org Chem 2011;76(15):6134–45.
[50] Kothavale S, Sekar N. Novel pyrazino-phenanthroline based rigid donor-π-acceptor compounds: a detail study of optical properties, acidochromism, solvatochromism and structure-property relationship. Dyes Pigments 2017;136:31–45.
[51] Achelle S, Rodríguez-López J, Bureš F, Robin-le Guen F. Tuning the photophysical properties of push-pull azaheterocyclic chromophores by protonation: a brief overview of a French-Spanish-Czech Project. Chem Rec 2020;20(5):440–51.
[52] Achelle S, Rodríguez-López J, Katan C, Robin-le Guen F. Luminescence behavior of protonated methoxy-substituted diazine derivatives: toward white light emission. J Phys Chem C 2016;120(47):26986–95.
[53] Dou C, Han L, Zhao S, Zhang H, Wang Y. Multi-stimuli-responsive fluorescence switching of a donor-acceptor π-conjugated compound. J Phys Chem Lett 2011;2 (6):666–70.
[54] Chen S, Qiu R, Yu Q, zhang X, Wei M, Dai Z. Boranil dyes bearing tetraphenylethene: synthesis, AIE/AIEE effect properties, pH sensitive properties and application in live cell imaging. Tetrahedron Lett 2018;59(27):2671–8.
[55] Kortekaas L, Lancia F, Steen JD, Browne WR. Reversible charge trapping in bis-carbazole-diimide redox polymers with complete luminescence quenching enabling nondestructive read-out by resonance Raman spectroscopy. J Phys Chem C Nanomater Interfaces 2017;121(27):14688–702.
[56] Lanke SK, Sekar N. AIE based coumarin chromophore - evaluation and correlation between solvatochromism and solvent polarity parameters. J Fluoresc 2016;26(2): 497–511.
[57] Prakasam M, Anbarasan PM. Second order hyperpolarizability of triphenylamine based organic sensitizers: a first principle theoretical study. RSC Adv 2016;6(79): 75242–50.
[58] Bhagwat AA, Sekar N. Fluorescent 7-substituted coumarin dyes: solvatochromism and NLO studies. J Fluoresc 2019;29(1):121–35.